CREEP RUPTURE PROPERTIES OF LAVES PHASE STRENGTHENED Fe-Ta-Cr-W AND Fe-Ta-Cr-W-Mo ALLOYS

Contents

CREEP RUPTURE PROPERTIES OF LAVES PHASE STRENGTHENED Fe-Ta-Cr-W AND Fe-Ta-Cr-W-Mo ALLOYS

Satbinder Singh
Materials and Molecular Research Division, Lawrence Berkeley Laboratory
and Department of Materials Science and Engineering,
Berkeley, California 94720

ABSTRACT

The small addition of tungsten (0.5at.%) was shown to have an effect similar to that of molybdenum on the phase transformation characteristics of alloy Ta7Cr (with a nominal composition of lat%Ta, 7at%Cr, balance Fe). The existance of time-temperature dependent transformation behavior in alloy Ta7Cr0.5W was confirmed.

The effect of spherodization time and temperature on creep strength was determined. In addition, effect of mechanical processing prior to aging, on creep strength was also determined. It was also shown that by suitable modifications of composition, the grain boundary film can be broken during the aging treatment without the use of spherodization treatment.

Microhardness, tensile and creep properties have been determined. Optical metallography and scanning electron microscopy have been used to follow the microstructural changes and mode of fracture. The creep rupture strength of alloy Ta7CrW alloy was found to be superior to many of the best commercially available ferritic alloys at 1200°F.

I. INTRODUCTION

In the past few years the possibility of developing iron-base alloys strengthened by intermetallic precipitates has received significant attention and studies of Fe-Ta, Fe-Nb and Fe-W alloys have been reported.[1-6] Such alloys contain a fine dispersion of Laves phase precipitates (Fe_2Ta, Fe_2Nb, etc). Most of these alloys also have a grain boundary film. The alloys containing Fe_2Nb and Fe_2Ta were found to have highest strength.[6] In Russel H. Jones' work,[6] the brittle fracture characteristic was eliminated by the use of simple $\alpha \rightarrow \gamma$ transformation which spherodized the continuous grain boundary network. However, the high solution treatment temperature required caused oxidation problem. Subsequent investigations[8] to determine the effect of chromium addition showed that ternary addition of chromium lowered the solution treatment temperature and increased the oxidation resistance considerably. The investigation indicated that the phase transformations and structural features of Fe-Ta-Cr alloys were similar to those of binary Fe-Ta alloys.[8] This created interest in the development of elevated temperature creep resistance alloys using a dispersion of Laves phase in a non-carbon containing body centered cubic iron matrix for applications in petroleum refineries, power generation equipment, aircraft engine components, etc.

Most commercially available creep resistant materials derive their strength from the dispersion of a second phase, which hinders the movement of dislocations and also retards recovery. In creep resistant ferritic steels, the dispersion invariably consisted of one or more types of carbides. The various problems associated with the use of dispersion of carbides for providing elevated temperature strength in

ferritic steels were discussed and it was suggested that many of these problems might be overcome by the use of dispersion of Laves phase compounds rather than carbides.[9] Subsequently, iron-base alloys with a dispersion of Fe-Ta Laves phase were developed. The good room and elevated temperature properties of a ternary alloy Ta7Cr (with a composition of lat.%Ta, 7at.%Cr and balance Fe) were reported.[10] The structural examination of alloy Ta7Cr after creep testing indicated partial recovery of dialocation substructure. Further investigations were carried out to retard recovery by solid solution strengthening. This led to the development of Ta7Cr0.5Mo Alloy (with a nominal composition of lat.%Ta, 7at.%Cr, 0.5at%Mo and balance Fe). The alloy Ta7CrMo had considerably higher rupture strength than alloy Ta7Cr and was better than many commercially used ferritic alloys.[11]

The objective of the present investigation was to develop and further improve the elevated temperature properties of ferritic alloys strengthened with the dispersion of Laves phase. The effect of W on improving the high temperature strength is well known.[12-16] As in the case of Mo, W was expected to retard recovery by solid solution strengthening. The effect of W on improving the high temperature properties was shown to be similar to that of Mo on an atomic basis.[16] Although some investigators[17] have shown that the combined effect of 0.5%Mo-0.5%W produced greater creep strength than 1%Mo or 1%W alone, other investigators[16] were not able to confirm this finding. It was of interest to investigate this problem with respect to high temperature strengthening effects of W and Mo in ferritic alloys strengthened with Laves phase. The study was carried out with two alloys of nominal composition

Fe-1at.%Ta-7at.%Cr-0.5at.%W and Fe-1at.%Ta-7at.%Cr-0.25at.%W-0.25at.%Mo. An examination of the phase transformation which occurred during spherodization heat treatment showed "C" curve kinetics similar to those in FeTaCrMo alloy. In FeTaCrW alloy some grain boundary films were already broken during aging treatment and thus good ductility was observed even without spherodization treatment.

Short term tensile properties of the alloys Fe1Ta7Cr0.5W and Fe1Ta7Cr0.25Mo0.25W were determined at the room temperature. Creep and stress rupture tests were carried out to determine creep and rupture strength of alloys Fe1Ta7Cr0.5W and Fe1Ta7Cr0.25W0.25Mo subjected to various heat treatment cycles. The resulta were compared with Ta7Cr alloy, Ta7Cr0.5Mo alloy and several commercial alloys. The creep rupture strength of Fe1Ta7Cr0.5W alloy (with only aging treatment) was found to be superior to many existing ferritic alloys with reasonable room temperature ductility.

II. EXPERIMENTAL PROCEDURE

A. Alloy Preparation and Processing

Alloys with chemical composition listed in Table 1 were cast from 99.95% purity electrolytic iron (GliddenA-104), 99.95% purity electrolytically deposited chromium and 99.9% purity Tantalum, Tungsten and Molybdenum rods. The compositions of Iron, Tantalum, Tungsten and Molybdenum used is given in Table II. Heats of approximately 10,300 grams were induction melted under the argon atmosphere, cast in heavy copper molds and annealed in vacuum for three days at 1100°C.

The ingots were forged at 1100°C into plates 3 in. by 9/16 in. in cross section. Creep specimen blanks 9/16 in. by 9/16 in. in cross section and 3 5/8 in. long were cut-out of these plates. For tensile specimen blanks the 9/16 in. thick plates were further reduced by rolling at 1100°C to a thickness of 7/32 in., and blanks 7/32 in. by 5/8 in. in cross section and 2 7/8 in. long were cut-out. To test the effect of cold work on creep properties of the alloys, the solution treated creep specimen blanks were further reduced by 50% and 70% and were cut to blanks of 3 4/5" X 4/5" X 5/32" for flat creep specimen.

B. Heat Treatments

The specimen blanks were surface ground to remove the oxide layer and were then encapsulated in evacuated and argon back-filled (0.3 atmospheric pressure of argon gas at room temperature) quartz tubes. The heat treating procedure consisted of one hour solution treatment at 1300°C followed by hot water (60°C) quenching. Next aging was carried at 700°C in molten salt bath followed by air cooling. For spherodization cycle, the blanks were enclosed in protective stainless steel bags

and were air cooled after each cycle. The solution treatment temperature and spherodization temperature and time was determined by metallographic techniques. The several different heat treatments are described in Table III.

C. Hardness Tests

Measurements of Vickers microhardness were made on metallographically polished and etched specimen using LEITZ miniload hardness tester using a diamond pyramid indentor and a load of 2000 grams. For each hardness measurement, at least six indentations were made.

D. Tensile Tests

The tensile properties of heat treated alloys were determined for flat specimens with a 1 in gauge length, 0.2 in. thickness and a width of 0.125 in. at the test section, were machined out of the tensile blanks. Figure 1 shows a sketch of the specimen. The specimens were loaded through aligning pins in the wide ends of the specimens. The tests were conducted at a strain rate of 0.04 per minute. The total elongation was measured between two fine scratch marks, one at each length of the gauge length. The 0.2% offset yield strength and ultimate tensile strength were determined from the chart record. The fracture surface was examined by the Scanning Electron Microscope at 25kV.

E. Creep and Stress Rupture Testing

Constant load creep and stress rupture tests were carried out on round specimens with threaded ends and a gauge section diameter of 0.25 in. A sketch of the specimen is shown in Fig. 2. The SATEC Model M-3 creep tester and specimen train assembled for testing has been previously described in detail.[10] Figure 3 shows the specimen train

assembly. Temperature of the specimen was measured by two thermocouples, one attached to each end of the specimen gauge section. The temperature gradient along the gauge section was less than 3°C throughout the test.

A similar method was used for testing the flat specimen. In this case the specimen were loaded through aligning pins in the wide end of specimen. A sketch of the specimen is shown in Fig. 4. Creep strains and rupture time was measured.

F. Structural Analysis

1. X-ray Analysis

Specimen for X-rays analysis were prepared by mechanical grinding followed by chemical polishing to remove the deformed layer resulting from mechanical grinding. A solution containing a 1:1 mixture of H_3PO_4 and H_2O_2 and a few drops of HF was used for chemical polishing. The specimens were examined in a Norelco X-ray diffractometer using CuK_α radiation and a crystal monochromator to reduce the fluorescent radiation.

2. Optical Metallography

Specimens were ground on emery papers and polished with 1.0 micron diamond paste and finally polished with 0.05 micron Al_2O_3 powder. Kalling's reagent (5 gms. $CuCl_2$, 100 ml each of HCl, C_2H_5OH and H_2O) was used as etchant. A Carl Zeiss Metallograph was used for examination of microstructures.

3. Scanning Electron Microscopy

JEOLCO JSM-U3 Scanning Electron Microscope was utilized to study the grain boundary and matrix precipitation morphology. Specimen were polished and overetched. The surface was tilted towards the incident beam.

Fracture surfaces of creep rupture specimens and tensile specimens were also examined in the scanning electron microscope.

III. RESULTS AND DISCUSSION

A. Phase Relations and Phase Transformation Behavior

Fe-Ta-Cr-W and Fe-Ta-Cr-W-Mo Alloys

The iron rich portion of the Fe-Ta binary phase diagram, which has been determined accurately by Sinha and Hume-Rothery[18] is shown in Fig. 5.

Previous investigators have shown that the Laves phase precipitates in Ta7Cr had interplanar spacings very nearly those of solid solution of Fe in Fe_2Ta approximating a composition Fe_2Ta_3 which lies within the range of composition predicted by Brewer[19] for the Laves phase in Fe-Ta alloys. The alloy Ta7Cr was modified by the addition of 0.5at.% of W and by addition of 0.25at.%W - 0.25at.% Mo. The binary Fe-W phase diagram[20] (Fig. 6) and binary Fe-Mo phase diagram[18] (Fig. 7) indicates that such small amount of W and Mo goes into solid solution in iron. A similar behavior can be expected for alloys FelTa7Cr0.5W and FelTa7Cr0.25W0.25Mo. X-ray diffraction also indicated that precipitates in these alloys had similar interplanar spacings as were obtained for precipitates for Ta7Cr alloy. Hence it can be concluded that as in the case of Ta7Cr alloy,[8] Fe_2Ta is the only stable phase in these alloys too.

The binary diagram, though, modified by additions of Cr, W & Mo, still, the general characteristics of the phase diagram remained same. The transformation behavior on heating the retained δ to the temperature in two phase $\gamma+Fe_2Ta$ was studied. The TTT diagram on heating was obtained by metallographic techniques discussed elsewhere.[11]

The alloys prior to transformations were solution treated at 1300°C for one hour and then quenched in hot water at 60°C. The microstructure

in quenched specimens consisted of large equiaxed grains (1 m.m. in diameter) of retained δ phase and continuous network of the Laves phase (Fe_2Ta) precipitates on the grain boundaries (Fig. 9a) and Fig. 9b). Figure 12 shows the scanning electron micrographs of spherodized FelTa7Cr 0.5W Alloy.

The $\delta \rightarrow \gamma + Fe_2Ta$ transformation in both FelTa7Cr -.5W and FelTa7Cr o.25Mo 0.25 W alloys exhibited 'C' curve kinetics similar to the Fe Ta Cr Mo alloy;[11] the nose of the finish curves for both the W and W-Mo alloy was located at 1000°C. Figure 13 shows the TTT diagram obtained for FelTa7Cr 0.5W alloy on heating the retained δ phase into the two phase $\gamma + Fe_2Ta$ region.

The possible explanations for possible 'C' curve behavior seen in these alloys on heating has recently been discussed.[11]

B. The Aging Characteristics - Micro-Hardness Results

The metallographic results indicated that a correlation existed between the changes in hardness and the amount of precipitate. The first hardness increase on aging were associated with the first detectable precipitation. The hardness increased continuously as further precipitation occurred until at the hardness peak almost equilibrium volume fraction of precipitates had formed. The hardness decrease after peak hardness had been reached, was primarily associated with increase in interparticle spacing due to solution of smaller particles and growth of larger ones to minimize the surface energy. Thus, the time required to reach peak hardness can be used as measure of the kinetics of the precipitation process.

The influence of temperature on the aging characteristics of FelTa7Cr 0.5W alloy when quenched from δ phase field is shown in Fig. 8. Normal influence of temperature, that is, the lower the temperature, the longer the time required to reach peak hardness. The peak hardness increases with decreasing aging temperature. Only a single aging peak is observed, which is consistent with the proposal that only a single precipitation process occurs.

A similar aging behavior was observed for the FelTa7Cr0.25Mo0.25W alloy. The peak hardness on aging at 700°C occurred in 90 minutes in both the alloys. The time and temperature was chosen for the aging heat treatment. In both the alloys the hardness observed was considerably higher than the ternary Ta7Cr alloy. This increase in hardness can be attributed to solid solution hardening effect by Tungsten and Molybdenum.

The aging characteristic of the alloy Ta7Cr0.25@0.25Mo was similar to that of Ta7Cr. The heat treatment consisted of a solution treatment in a single δ phase region at 1300°C for 1 hour, quenching in hot water, followed by aging at 700°C. Figure 10 shows the optical micrograph of the alloy at peak hardness. Continuous network of precipitates were present before aging reaction (Fig. 9). This continuous network was formed during quench from solution treating temperature. Aging at 700°C resulted in precipitation of the Laves phase within the grains.

In alloy Ta7Cr 0.5W, also, the continuous network of precipitate were formed during quench from the solution treating temperature. But during aging reaction some grain boundaries films broke down. Figure 11 shows the Scanning Electron Micrograph of the aged specimen. The Tungsten

like chromium seemed to have changed the surface energy, thus causing spherodization of some matrix particles and grain boundary precipitates during aging treatment. The precipitate size varied widely in diameter. Some of the particles were as small as 0.03 μ whereas particles as big as 4 μ were also observed (Figs. 11-12).

C. Tensile Properties

Short time tensile tests at room temperature were conducted on flat tensile specimens of alloys Ta7Cr 0.5W and Ta7Cr 0.25W 0.25Mo subjected to various heat treatments. The results obtained are listed in Table IV.

The spherodization treatment considerably enhanced the yield strength over the aged alloys. No significant change in room temperature tensile strength was observed by changing spherodization time or temperature. Normally, the tensile properties of dispersion strenghtened alloys are influenced by heat treating procedures, as it changes the size and dispersion of dispersed phase. But differences in room temperature tensile properties in these alloys resulting from different thermal treatments were small. It seems that precipitate morphology and distribution did not have significant influence on short time tensile properties, and the nature of the matrix was more important.

It has been seen by transmission electron microscopy of thin foil specimen of alloy Ta7Cr, which was subjected to the $\delta \leftrightarrow \gamma$ spherodization cycle that substructure established within the grains were characterized by high dislocation density.[10] A similar behavior was expected in quarternary alloy Ta7Cr 0.5W and alloy Ta 7 Cr 0.25W 0.25 Mo subjected to $\delta \leftrightarrow \gamma$ spherodization thermal treatment. The increase in yield strength of spherodized alloys over the aged alloys at room temperature may be

attributed to this high dislocation density and small grain size.

The room temperature tensile properties obtained in both the alloys studied were comparable. The good ductility obtained in the aged alloys can be attributed to the broken grain boundary films in aged alloys itself. The Tungsten, like Chromium seemed to have changed the surface energy, thus causing some spherodization of grain boundary and matrix particles during the aging treatment and thus, improvement in room temperature ductility.

The large precipitate free zone seen in the FelTa7Cr 0.25Mo 0.25W alloy didn't seem to have adverse effect on room temperature properties of the alloys. But it had drastic effect on the creep properties of the alloy as discussed in the next section.

B. Stress Rupture Properties

1. Stress Rupture Properties of Alloy Ta 7 Cr MoW

Constant load stress rupture tests were conducted at 1100°F (593°C) and 1200°F (649°C) on the alloy FelTa7Cr0.25Mo0.25W. Results of the stress rupture tests for this alloy are listed in Table V. The creep strength of chis alloy at both 1100°F and 1200°F were lower than those of FelTa7Cr 0.5 Mo, and FelTa7Cr 0.5W alloy, but were higher than those of FelTa7Cr alloy.

Microstructural examination showed that there is a very large precipitate free zone adjacent to the grain boundaries. The poor creep properties of the alloy can be attributed to this large precipitate free weak zone (Fig. 14). The microhardness results confirmed that the precipitate free zone close to grain boundaries is a soft area.

Attempts were made to improve the creep properties by reducing or

eliminating this precipitate free zone by cold working prior to aging. The solution treated specimen (1/2" thick) were cold rolled to 1/4" thick strips in four passes. These were then aged at 700°C for 90 minutes before spherodization treatment. This treatment resulted in considerable reduction in the precipitate free zone and also in finer precipitate particles (Fig. 15). The microhardness value also increased from 200 V.H.N. in conventional aged specimen to about 310 V.H.N. in cold worked and aged specimen. But the improvement in creep properties were marginal. This was surprising as reduction in precipitate free zone and finer precipitate size are expected to enhance the creep strength. The probable reason for not getting expected improvement in the creep properties in cold work specimen lies in the grain size. The prior cold work resulted in extremely fine grain size on spherodization, and fine grain size is not good for the creep strength at high temperatures.

Whereas Colbeck and Rait found a creep-strengthening advantage in adding molybdenum and tungsten in combination rather than either alone,[17] while such an interaction effect in creep resistance may well be detected for molybdenum and tungsten, this synergestic effect was not evident in the rupture tests of this investigation.

2. Stress Rupture Properties of Alloy Ta7CrW

As in the case of Ta7CrMoW alloy, the stress rupture tests for alloy Ta7CrW was conducted at 1100°F(593°C) and 1200°F(649°C) for a variety of heat treatments. The results of these tests are listed in Table VI(a) and Table VI(b). The rupture time with spherodization heat treatment resulted in creep strength slightly lower than reported for Ta7CrMo alloy, but with slightly superior tensile properties. The heat treatment T-3

resulted in best tensile properties and best creep properties in case of spherodization heat treatment. Some tests were also run in directly spherodized alloy, without the aging treatment. This resulted in lower creep strength compared with aged and spherodized alloys. This can be explained on the basis of precipitate size and distribution. Even though in both, aged and spherodized and spherodized directly specimen, overaging occurs, the initial precipitation at lower temperatures results in finer precipitates, which doesn't grow as fast as the precipitates formed at higher aging temperatures. Therefore, three step heat treatment results in superior creep properties.

Effect of spherodization time and temperature on rupture life was studied. It was seen that as the spherodization temperature was raised, spherodization time in each case being the time required for just completion of $\delta \rightarrow \gamma$ transformation, the rupture life increased as shown in Fig. 16. Similarly, when spherodization time was increased at different spherodization temperatures, the rupture life increased with the spherodization time. Figure 17 shows the effect of spherodization time on rupture strength at 1200°F at stress of 20,000 p.s.i. The spherodization temperature was 1000°C. The best creep properties in case of spherodization heat treatment were obtained by spherodization at highest possible temperature, at which $\delta(\alpha) \rightarrow \gamma$ transformation occurs, for longest period of time. The reason for this was attributed to the increase in grain-size as the temperature and time of spherodization is increased. This is further confirmed by the results obtained by cold worked and then aged and spherodized specimen. Even though this specimen showed higher hardness values, its creep properties were poor, indicating that large

grain size is beneficial for the creep strength at 1100°F and 1200°F for this alloy.

The examination of alloy Ta7Cr0.5W, aged to peak hardness, under the scanning electron microscope indicated that some of the continuous network of precipitates formed at grain boundaries during quenching were broken during the aging treatment, which resulted in further precipitation within the grains. Therefore, it was expected that in this alloy, reasonable room temperature ductility should be observed along with good creep strength in aged condition itself without any need for the spherodization treatment.

The results obtained confirmed this. The Ta7CrW alloy with the aging treatment only, did not rupture in 1000 hours at 1200°F under the stress of 17000 p.s.i. It's yield strength was 51,000 p.s.i. and tensile strength was 87,000 p.s.i. with 15.5 percent elongation in 1" gauge length. The creep and rupture strength was better than those of alloy Ta7CrMo and several ferritic steels at 1200°F.

This showed that it is possible to break the continuous film forming at grain boundaries not only by spherodization heat treatment but also by the suitable composition adjustments. The advantage of latter over the former is that, since very high temperature treatment is eliminated, overaging is avoided, further the spherodization treatment after aging results into finer grain size due to $\delta(\alpha)^{*}\gamma$ phase transformation involved, which is not good for creep strength at high temperatures.

The alloy Ta7Cr0.5W confirmed that advantages of breaking the grain boundary film by composition modifications. Even though the grain boundaries films were not broken completely in this alloy, it showed reasonably good

room temperature properties with excellent creep rupture strength as compared to spherodized alloys of the same composition. Thus, if by further composition modifications all the grain boundary films could be completely broken, without the need for spherodization treatment, an alloy with excellent room temperature properties along with outstanding creep properties for applications at elevated temperatures of around 600°C, could be developed.

E. Fracture Characteristics

For aged Ta7Cr0.5W alloy, the scanning electron microscope pictures of fracture surface of tensile specimen consisted of a combination of river and cup and cone patterns (Fig. 18). The dual nature of the fracture surface may be due to the partly broken film of grain boundary precipitates (Fig. 11). For the spherodized specimen, dimpled rupture, characteristic of ductile fracture, was observed (Fig. 19).

The fracture surfaces of alloy Ta7Cr0.5W, tested to rupture at 1100°F and 1200°F at different stress levels were also examined in the scanning electron microscope. In Fig. 20 and 21 is shown the fracture morphology of specimens with treatment T-4 & T-7 ruptured at 1200°F at stresses 17000 p.s.i. and 20,000 p.s.i. respectively. The fracture characteristics of completely ductile material was observed. The fracture was initiated by failure of precipitate matrix interfaces, which resulted in the formation of voids. The ductile tearing which resulted in the final failure occurred after the formation of a large number of voids.

The aged specimen was not examined under the microscope as it did not rupture during the creep tests.

The fracture characteristics of Ta7Cr0.25Mo0.25W was similar to the

Ta7Cr0.5W alloy in case of spherodized specimen. In this alloy initiations of fracture at grainboundaries was observed, confirming that precipitate free zone at grain boundaries are weak area, where the specimen fails.

IV. SUMMARY AND CONCLUSIONS

The phase transformation characteristics of FelTa7Cr0.5 W alloy and FelTa7Cr0.25Mo0.25W alloy were shown to be similar to FelTa7Cr0.5Mo alloy. A study of phase transformation behavior of alloy Ta7Cr0.5W and Ta7Cr0.25Mo 0.25W indicated the existance of a temperature time dependent transformation on heating similar to Ta7Cr0.5Mo alloy reported elsewhere.[11]

The aging characteristics of both the alloys were shown to be similar to binary Fe-Ta alloy. The peak hardness observed was considerably greater than that seen for ternary FelTa7Cr alloy. The grain boundaries in aged FelTa7Cr0.5W alloys were not completely continuous. This resulted in improved room temperature properties in Ta7CrW alloy without the use of spherodization treatment. The tensile properties of spherodized alloys were superior to FelTa7Cr 0.5 Mo alloys.

The alloy FelTa7Cr0.25W0.25Mo didn't show the expected synergestic effect of Mo-W. The alloy FelTa7Cr0.5W had superior creep strength as compared with FelTa7Cr0.25Mo 0.25W alloy. The Ta7Cr0.5W alloy in spherodized condition had slightly lower creep strength than Ta7Cr0.5Mo alloy but superior room temperature tensile and yield strength.

It was shown that creep strength of the alloys increased with increase in spherodization time and temperature. It was shown that larger the grain size, better the creep properties are at 1100°F and 1200°F for these alloys. It was also shown that prior cold work before aging doesn't result in the improvement of stress rupture strength.

The creep strength of Ta7Cr0.5W alloy in aged condition was better than many of the best commercially used ferritic alloys at both 1100°F

and 1200°F (593° and 649°C). The stress rupture strength was higher than 403, 410 stainless steel, Greek Ascoloy, 0.3C-1Cr-1Mo-2.5V steel and 422 stainless steel at 1200°F.

The fracture surfaces of creep rupture specimen (with spherodization treatment) showed the fracture occurred by nucleation and growth of voids around particles of Laves phase precipitate leading to failure characterized by dimpled fracture appearance. The fracture surface of FelTa7Cr0.5W specimen in aged condition tested at room temperature showed dual character of ductile and brittle failure.

ACKNOWLEDGEMENTS

The author is deeply grateful to Professor Victor F. Zackay and Professor Earl R. Parker for their constant encouragement and guidance throughout the course of this investigation. He would also like to extend his appreciation to Professor I. Finnie for a review of the manuscripts. Special thanks are extended to Mr. M. S. Bhat and Dr. Dilip Bhandarkar for their constant help and many invaluable discussions.

The assistance provided by the technical support staff of the Materials and Molecular Research Division is acknowledged; thanks are due in particular, to John Holthuis (Alloy Processing), Lee Johnson (Metallography), Don Krieger (Mechanical Testing), Richard Lindberg (Scanning Electron Microscopy), Phila Witherell (Technical Photography), Gloria Pelatowski (Preparation of line drawing) and Gay Brazil (Manuscript preparation).

This work was done under the auspices of the U. S. Energy Research and Development Administration through the Materials and Molecular Research Division of the Lawrence Berkeley Laboratories.

REFERENCES

1. G. R. Spiech, Trans. A.I.M.E. 224, 1962 p. 850.
2. R. D. Rawling and C. W. A. Newey, Trans. A.I.M.E. 242, 1966, p. 1551.
3. R. M. Forbes Jones and D. R. F. West, J151, 208, 1970, p. 270.
4. Russel H. Jones, V. F. Zackay and E. R. Parker, Met. Trans. 3, 1972 p. 2835.
5. D. H. Jack and R. W. Honeycombe, Acta Met. 20, 1972, p. 787.
6. Russel H. Jones, E. R. Parker and V. F. Zackay in "Electron Microscopy and Structure of Materials", Ed. G. Thomas, University of California, Berkeley, 1972, p. 829.
7. G. Sasaki, Mechanical Properties of Laves Phases, Dec. 1970, University of California, Berkeley, Lawrence Radiation Laboratory, UCRL-20301.
8. S. Jin, M. S. Thesis, LBL Rep. 443, University of California, Berkeley, December, 1971.
9. V. F. Zackay, E. R. Parker and D. Bhandarkar, Proc. John E. Dorn Memorial Symposium on Rate Processes in Plastic Deformation, Cleveland, Ohio, October 1972. Also LBL-1174, Lawrence Berkeley Laboratory, October, 1972.
10. M. D. Bhandarkar, Structure and Elevated Temperature Properties of Ferritic Alloys Strengthened by Intermetallic Compounds (D. Eng. Thesis), LBL-1858, September 1973.
11. M. S. Bhat, M. S. Thesis, LBL Rep. 2277, University of California, Berkeley, California, April 1974.
12. C. R. Austin, C. R. St. John and R. W. Lindsay, Trans. Met. Soc. A.I.M.E., 162, 84 (1945).

13. S. F. Reiter and W. R. Hibbard, Jr., Trans. Met. Soc. A.I.M.E. 203, 655 (1955).

14. G. A. Mellor and S. M. Barker, J. Iron Steel Inst. 194, 464 (1960).

15. B. B. Argent, M. N. van Niekert and G. A. Redford, J. Iron Steel Inst. 208, 830 (1970).

16. A. E. Powers, Trans. A.I.M.E. 208, 1373 (1956).

17. E. W. Colbeck and J. R. Rait, Creep Resistant Ferritic Steels, Special Report No. 43, 1951, Iron and Steel Institute, London, p. 107.

18. A. K. Sinha and W. Hume-Rothery, J. Iron and Steel Inst., 205, p. 671 (1967).

19. L. Brewer, High Strength Materials, V. F. Zackay, ed., (John Wiley and Sons, Inc., New York (1965) p. 12.

20. Metals Handbook, Taylor Lyman, ed. (Amer. Soc. Metals, Ohio, 1973) Vol. I.

Table I. Chemical Compositions of Alloys

Alloy Designation	Compositions									
	Wt. Pct.					At. Pct.				
	Ta	Cr	W	Mo	Fe	Ta	Cr	W	Mo	Fe
Ta7 Cr W	3.4	6.32	1.63	-	Bal.	1	7	0.5	-	Bal.
Ta 7Cr W. Mo	3.16	6.35	0.80	0.42	Bal.	1	7	0.25	0.25	Bal.

Table II. Typical Purity of Starting Materials. Iron, Chromium, Tungsten and Molybdenum.

	Iron	Tantalum	Tungsten	Molybdenum
Ap	.001	-	-	-
Be	.0005	-	-	-
Ca	.001	.003	.008	-
C	.002	.004	.01	0.01
Cr	.001	-	-	-
Co	.001	-	-	-
Cu	.004	-	-	-
Fe	-	.003	.01	.02
H	.01	.001	.0002	-
Pb	.001	-	-	-
Mg	.0005	.006	.005	-
Mn	.0015	-	.005	-
Mo	.004	.02	.02	-
Nb	-	0.10	.005	-
Ni	.001	-	0.01	.01
N	.004	.004	.005	.001
O	.04	.005	.01	.003
P	.002	-	-	-
Si	.003	.003	.01	.01
S	.003	-	-	-
Ta	.001	-	-	-
Ti	-	-	0.005	-
Sn	.003	-	-	-

Table II. (Con't.)

	Iron	Tantalum	Tungsten	Molybdenum
W	.001	.05	-	-
V	.001	-	-	-
Zn	.001	-	-	-
Zr	-	.005	-	-

Table III. List of the heat treatments and their designation.

Heat Treatment	Designation
Solution treat at 1300°, 1 hr (ST) → hot water quench (HWQ) → age at 700°C, 1 1/2 hr (A) → air cool (AC).	T-1
ST → HWQ → Sperodize at 1050°C 90 minutes (t,1050°C, 90 Mrs) → AC	T-2
ST → HWQ → A → AC → S, 1075°C, 2 hr → AC	T-3
ST → HWQ → A → AC → S, 1075°C, 1 hr → AC	T-4
ST → HWQ → A → AC → S, 1050°C, 2 hr → AC	T-5
ST → HWQ → A → AC → S, 1050°C, 1 1/2 hr → AC	T-6
ST → HWQ → A → AC → S, 1050°C, 1 hr → AC	T-7
ST → HWQ → A → AC → S, 1000°C, 2 hr → AC	T-8
ST → HWQ → A → AC → S, 1000°C, 1 1/2 hr → AC	T-9
ST → HWQ → A → AC → S, 1000°C, 1 hr → AC	T-10
ST → HWQ → A → AC → S, 1000°C, 3/4 hr → AC	T-11
ST → HWQ → A → AC → S, 950°C, 2 hr → AC	T-12
ST → HWQ → Cold Work, 50% reduction → A → AC → S, 1050°C, 1 hr → AC	T-13

Table IV. Room Temperature Mechanical Properties

Alloy	Heat Treatment	Yield Strength Psi	Ultimate Tensile Strength Psi	Fracture Elongation, Pct.
Ta7CrW	T-1	51,200	86,400	16.5
	T-3	79,400	92,100	15
Ta7CrMoW	T-1	52,000	92,000	15.5
	T-3	77,500	92,000	15.8

Table V(a). Stress rupture properties of alloy Ta7CrMoW at 1100°F.

Heat Treatment	Stress (psi)	Rupture Time (hrs)
T-2	35,000	5.4
T-2	17,000	78.0
T-3	17,000	101.0
T-13	17,000	69.0

Table V(b). Stress rupture properties of alloy Ta7CrMoW at 1200°F.

Heat Treatment	Stress (psi)	Rupture Time (hrs)
T-2	17,000	10
T-4	17,000	23
T-5	17,000	14
T-13	17,000	17

Table VI(a). Stress rupture properties of alloy Ta7Cr0.5W at 1100°F.

Heat Treatment	Stress (psi)	Rupture Time (hrs)
T-2	25,000	176.0
T-2	35,000	19.5
T-5	25,000	182

Table VI(b). Stress rupture properties of alloy Ta7Cr0.5W at 1200°F.

Heat Treatment	Stress (psi)	Rupture Time (hrs)
T-1	17,000	did not rupture in 1000 hrs.
T-2	20,000	15.0
T-3	17,000	172.0
T-4	17,000	100.0
T-7	20,000	14.0
T-7	17,000	64.0
T-8	17,000	28.0
T-9	17,000	14.5
T-10	17,000	9.0
T-11	17,000	22.0
T-11	20,000	8.0
T-12	20,000	4.0
T-12	17,000	9.0
T-13	17,000	40.0

Table VIII. Rupture time at a stress of 15,000 psi at 1200°F (649°C) for alloys Ta7CrW, Ta7CrMo and some commercial ferritic steels.

Alloy	Rupture time for a stress of 15,000 psi (hr)	Reference
Ta7CrW	> 1000	Present Work
Ta7CrMo	682	11
0.3C-1Cr-1Mo-0.25V Steel	≈ 400	20
0.15C-9Cr-1Mo Steel	< 10	20
0.15C-7Cr-0.5Mo Steel	< 10	20
403,410 Stainless Steel	< 1	20
Greek Ascoloy	~ 190	20
422 Stainless Steel	~ 560	20

FIGURE CAPTIONS

Fig. 1. Schematic diagram of sheet tensile specimen used for room temperature tensile tests.

Fig. 2. Sketch of creep specimen used for creep, stress-rupture testing.

Fig. 3. Sketch of specimen and extensometer assembly used in creep and stress rupture tests.

Fig. 4. Sketch of the flat creep specimen used for stress rupture testing.

Fig. 5. The iron-rich portion of the equilibrium diagram of the Fe-Ta system.

Fig. 6. Equilibrium diagram of the iron-tungsten system.

Fig. 7. Equilibrium diagram of the iron-molybdenum system.

Fig. 8. The variation of room temperature microhardness of alloy Ta7CrW with aging time at 700°C and 800°C.

Fig. 9. (a),(b) Optical micrograph of alloy Ta7CrW in the solution treated condition.

Fig. 10. Optical micrograph of alloy Ta7CrW aged to peak hardness (heat treatment T-1).

Fig. 11. (a),(b). Scanning electron micrograph of alloy Ta7CrW aged to peak hardness (heat treatment T-1).

Fig. 12. Scanning electron micrograph of alloy Ta7CrW, completely spherodized (heat treatment T-3).

Fig. 13. Time Temperature Transformation curve for heating reactions of alloy Ta7Cr0.5W.

Fig. 14. Optical micrograph of alloy Ta7CrW Mo showing precipitate free zone close to grain boundaries (Heat treatment T-6).

Fig. 15. Optical micrograph of alloy Ta7CrW Mo (Heat treatment T-13).

Fig. 16. Rupture life at 1200°F at stress of 20,000 psi and 17,000 psi vs. spherodization temperature.

Fig. 17. Rupture life at 1200°F vs. spherodization tine at a stress of 20,000 psi. Temperature of spherodization is 1000°C.

Fig. 18. Scanning Electron fractograph of alloy Ta7CrW, aged to peak hardness and tested at room temperature (Heat treatment T-1).

Fig. 19. Scanning electron fractograph of alloy Ta7CrW tested at room temperature (heat treatment T-3).

Fig. 20. Scanning electron fractograph of alloy Ta7CrW, tested at 1200°F at a stress of 17,000 psi (heat treatment T-4).

Fig. 21. (a),(b) Scanning electron fractograph of alloy Ta7CrW tested at 1200°F at a stress of 20,000 psi (heat treatment T-7).

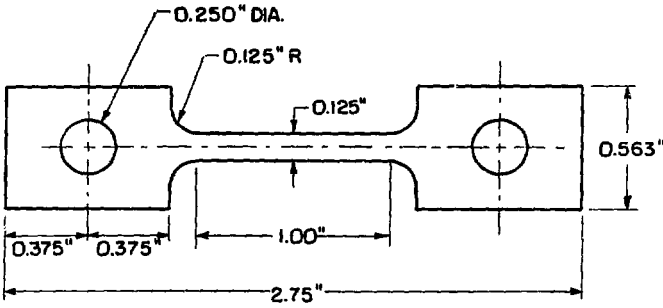
0.250" DIA.
0.125" R
0.125"
0.563"
0.375"
0.375"
1.00"
2.75"
THICKNESS = 0.20"
XBL737-6444

Fig. 1

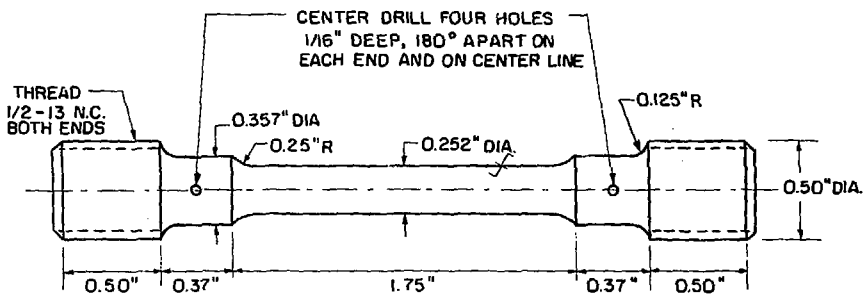
CENTER DRILL FOUR HOLES
1/16" DEEP, 180° APART ON
EACH END AND ON CENTER LINE
THREAD
1/2-13 N.C.
BOTH ENDS
0.357" DIA
0.25"R
0.252" DIA.
0.125"R
0.50"DIA.
0.50"
0.37"
1.75"
0.37"
0.50"
THE 0.252" DIA. REDUCED SECTION
SHOULD BE TAPERED 0.002"
TOWARD THE CENTER
FINISH 16 V ON
SURFACE
XBL737-6445

Fig. 2

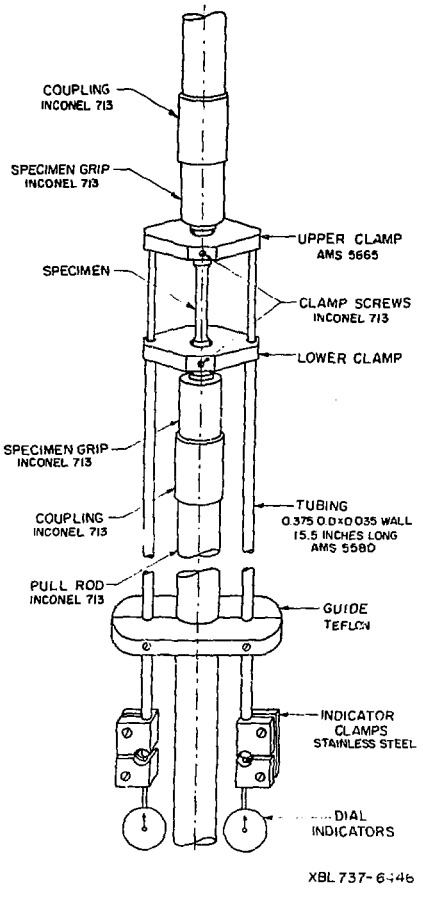
COUPLING
INCONEL 713
SPECIMEN GRIP
INCONEL 713
UPPER CLAMP
AMS 5665
SPECIMEN
CLAMP SCREWS
INCONEL 713
LOWER CLAMP
SPECIMEN GRIP
INCONEL 713
COUPLING
INCONEL 713
TUBING
0.375 O.D.×0.035 WALL
15.5 INCHES LONG
AMS 5580
PULL ROD
INCONEL 713
GUIDE
TEFLON
INDICATOR
CLAMPS
STAINLESS STEEL
DIAL
INDICATORS
XBL 737-6446

Fig. 3

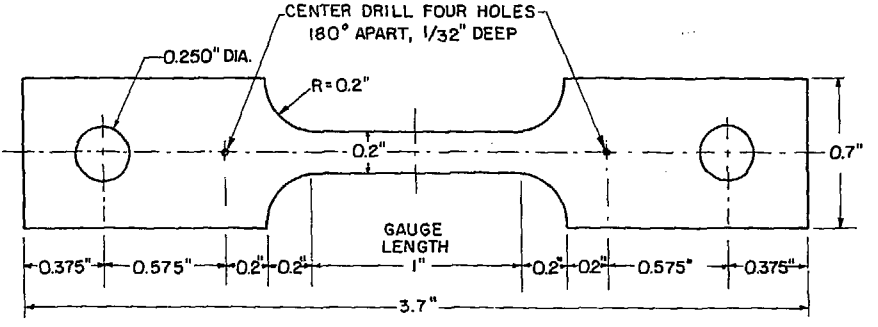

THICKNESS = 0.125"

XBL 7512-9259

Fig. 4

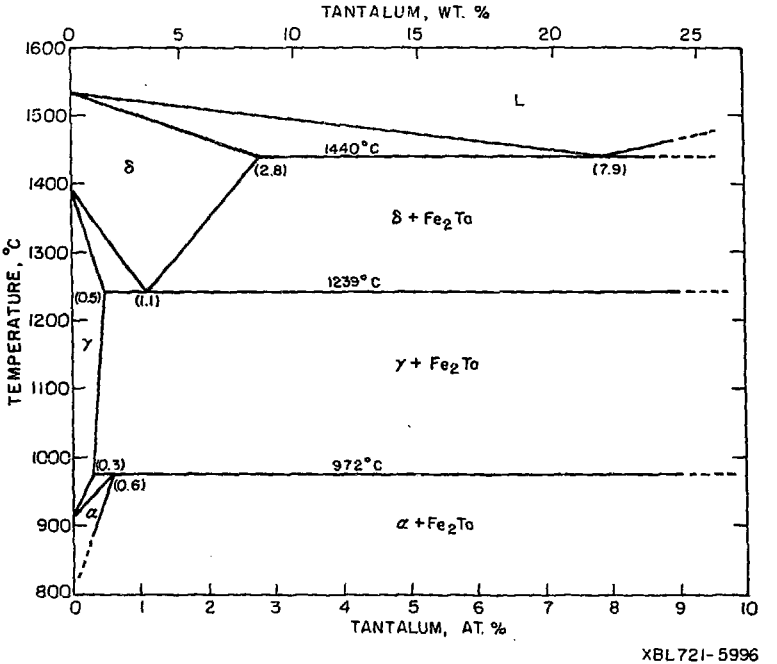

XBL721-5996

Fig. 5

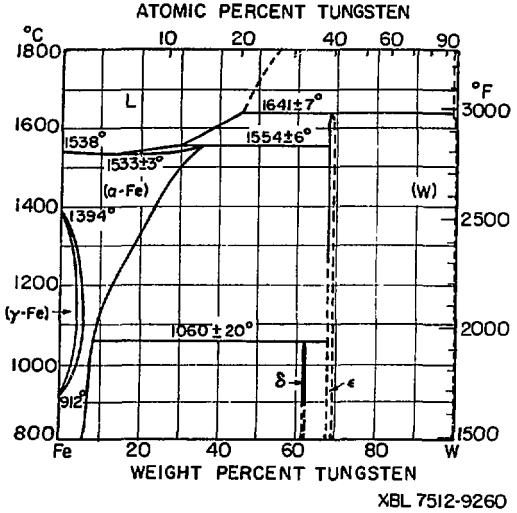
ATOMIC PERCENT TUNGSTEN
°C
°F
10
20
40
60
90
1800
1600
1400
1200
1000
800
3000
2500
2000
1500
L
1641±7°
1554±6°
1538°
1533±3°
(α-Fe)
(W)
1394°
(γ-Fe)
1060±20°
δ
ε
912°
Fe
20
40
60
80
W
WEIGHT PERCENT TUNGSTEN
XBL 7512-9260

Fig. 6

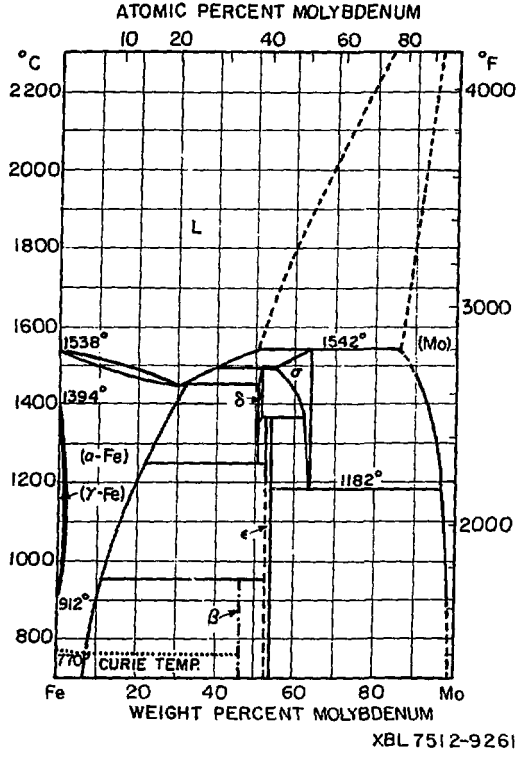
ATOMIC PERCENT MOLYBDENUM
10
20
40
60
80
°C
°F
2200
2000
1800
1600
1400
1200
1000
800
4000
3000
2000
L
1538°
1542°
(Mo)
σ
1394°
δ
(α-Fe)
(γ-Fe)
1182°
ε
912°
β
770°
CURIE TEMP.
Fe
20
40
60
80
Mo
WEIGHT PERCENT MOLYBDENUM
XBL 7512-9261

Fig. 7

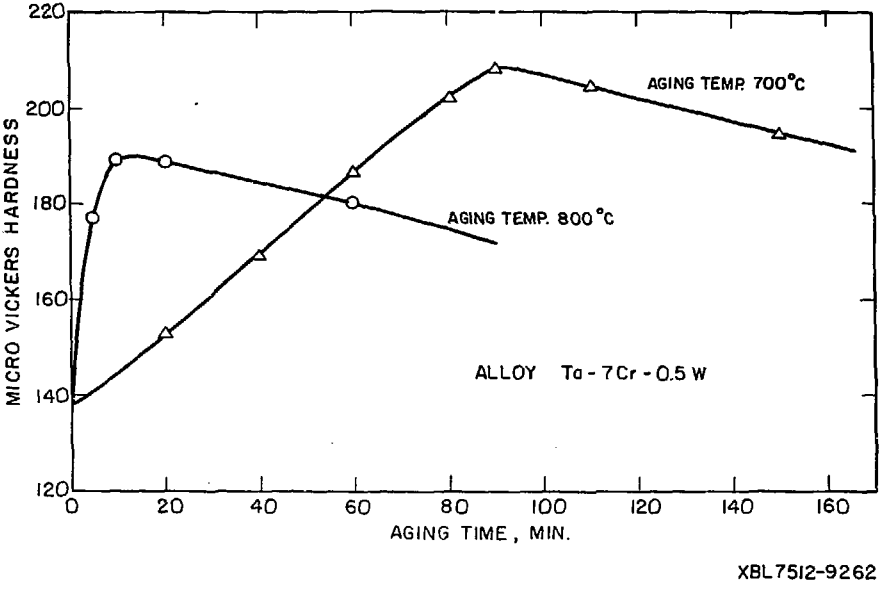
220
200
180
160
140
120
MICRO VICKERS HARDNESS
0
20
40
60
80
100
120
140
160
AGING TIME, MIN.
AGING TEMP. 700°C
AGING TEMP. 800°C
ALLOY Ta - 7Cr - 0.5 W
XBL7512-9262

Fig. 8

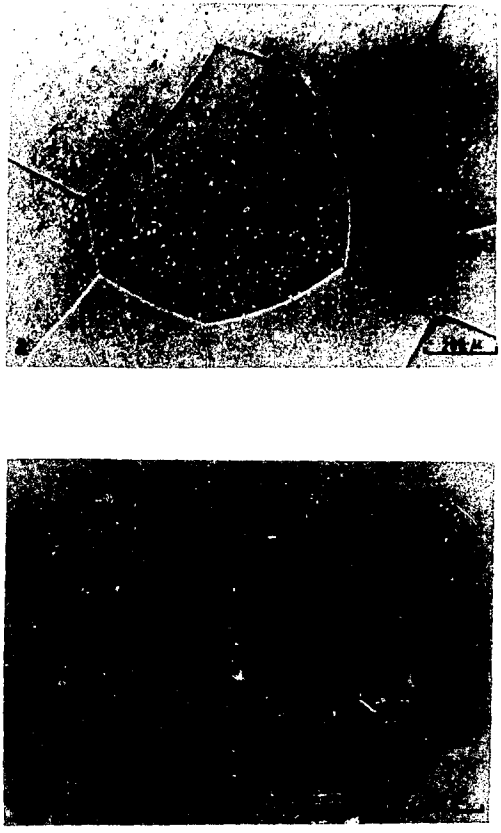

XBB 7512-9014

Fig. 9

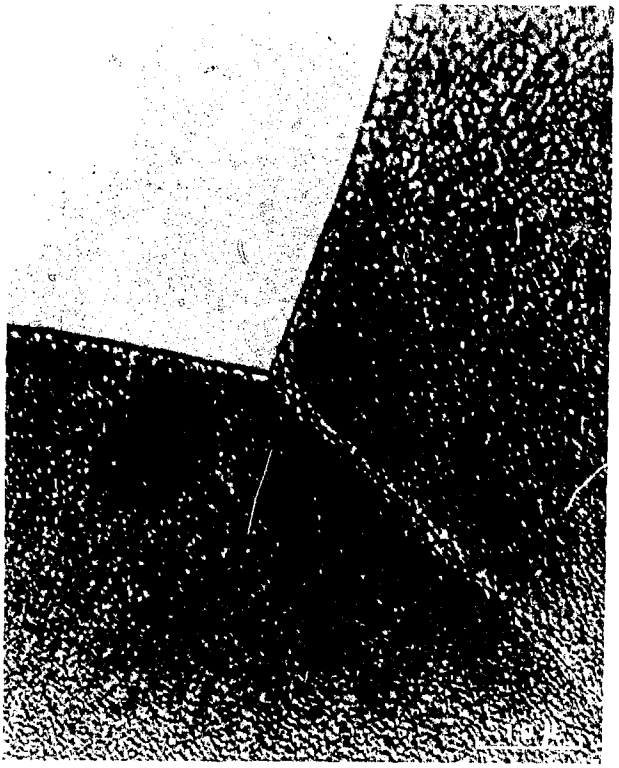

XBB 7512-9011

Fig. 10

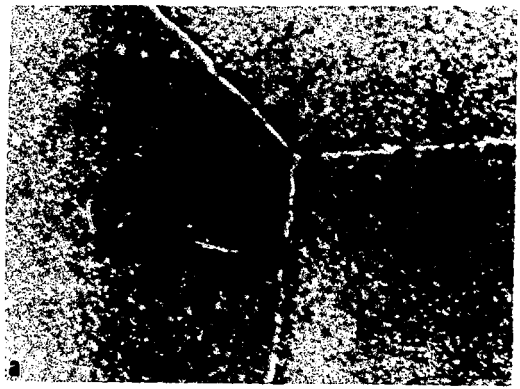

XBB 7512-9015

Fig. 11

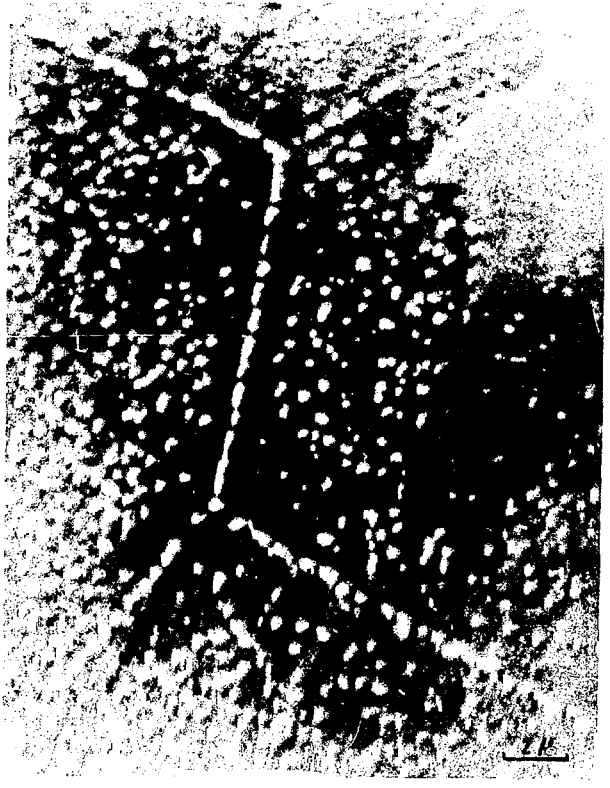

XBB 7512-9012

Fig. 12

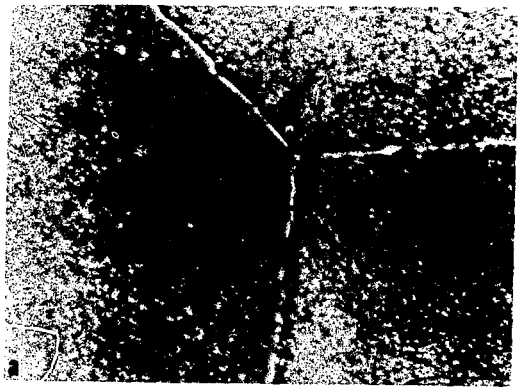

XBB 7512-9015

Fig. 11

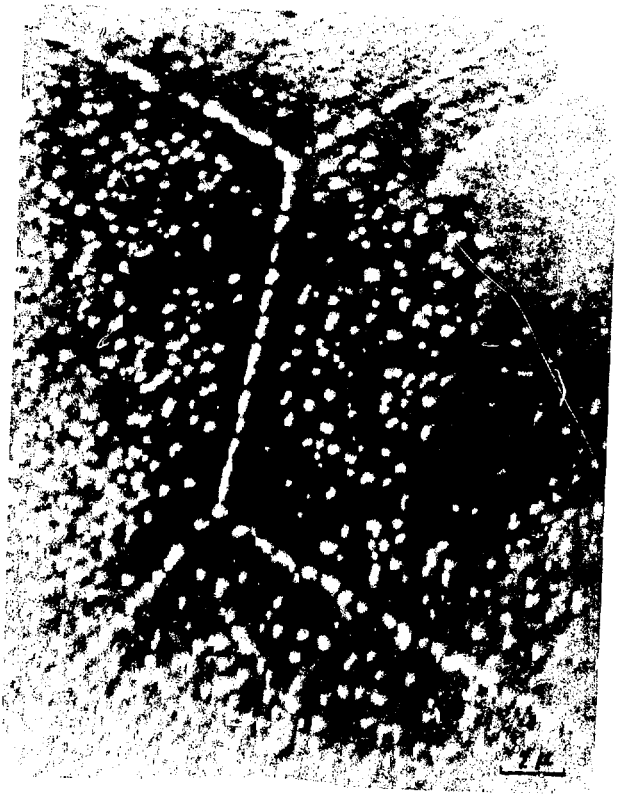

XBB 7512-9012

Fig. 12

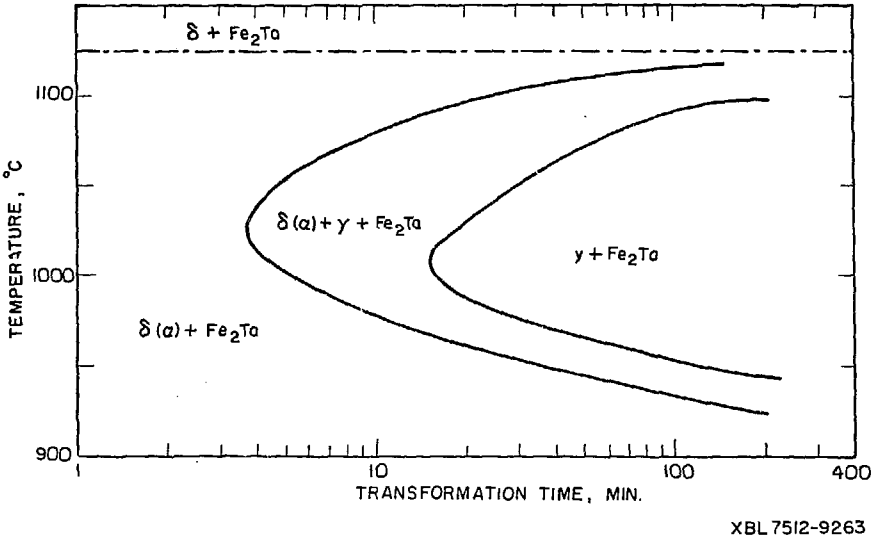
δ + Fe2Ta
1100
1000
900
TEMPERATURE, °C
δ (α) + γ + Fe2Ta
γ + Fe2Ta
δ (α) + Fe2Ta
1
10
100
400
TRANSFORMATION TIME, MIN.
XBL 7512-9263

Fig. 13

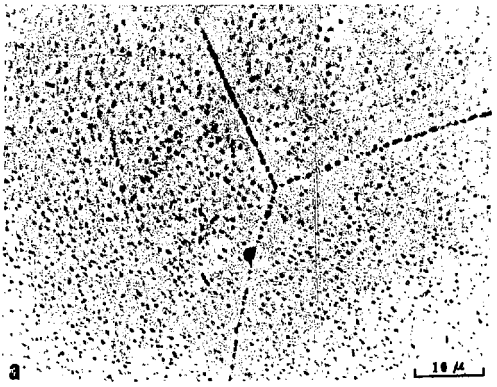

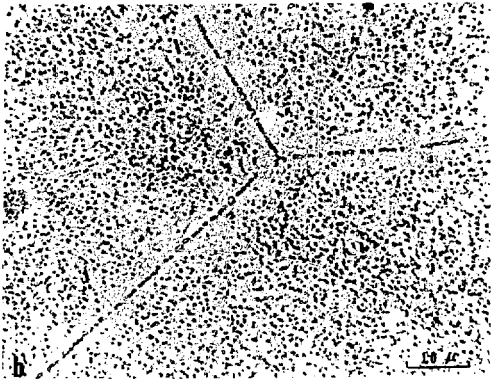

XBB 7512-9016

Fig. 14

XBB 7512-9010

Fig. 15

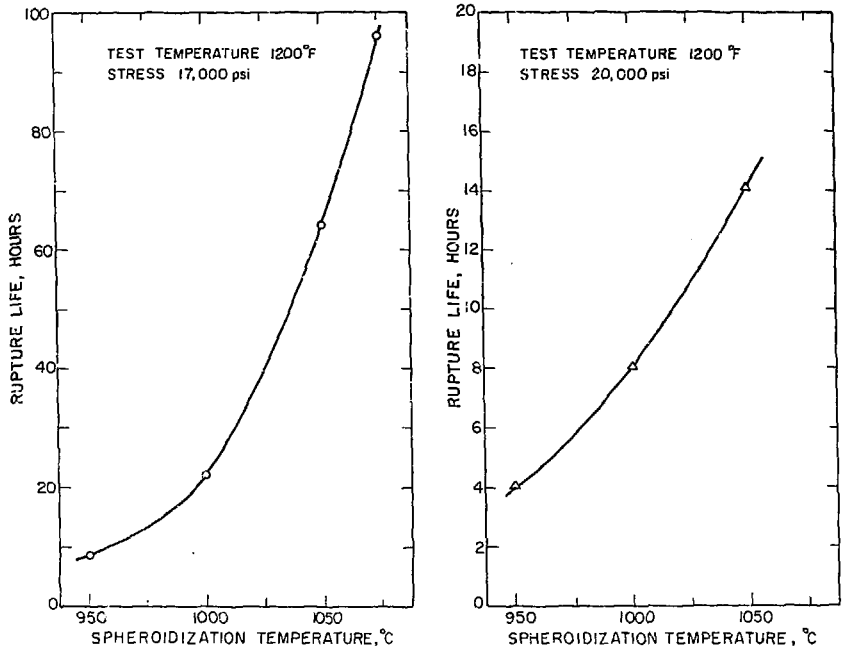
TEST TEMPERATURE 1200°F
STRESS 17,000 psi
RUPTURE LIFE, HOURS
SPHEROIDIZATION TEMPERATURE, °C
TEST TEMPERATURE 1200 °F
STRESS 20,000 psi
RUPTURE LIFE, HOURS
SPHEROIDIZATION TEMPERATURE, °C
XBL7512-9264

Fig. 16

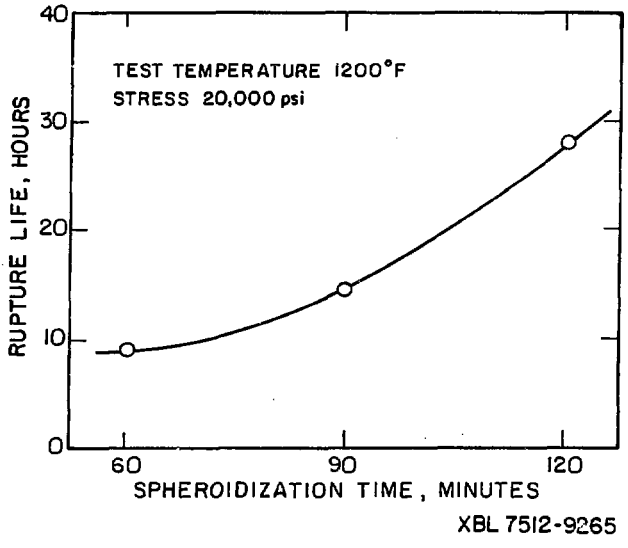
TEST TEMPERATURE 1200°F
STRESS 20,000 psi
RUPTURE LIFE, HOURS
0
10
20
30
40
60
90
120
SPHEROIDIZATION TIME, MINUTES
XBL 7512-9265

Fig. 17

XBB 7512-9009

Fig. 18

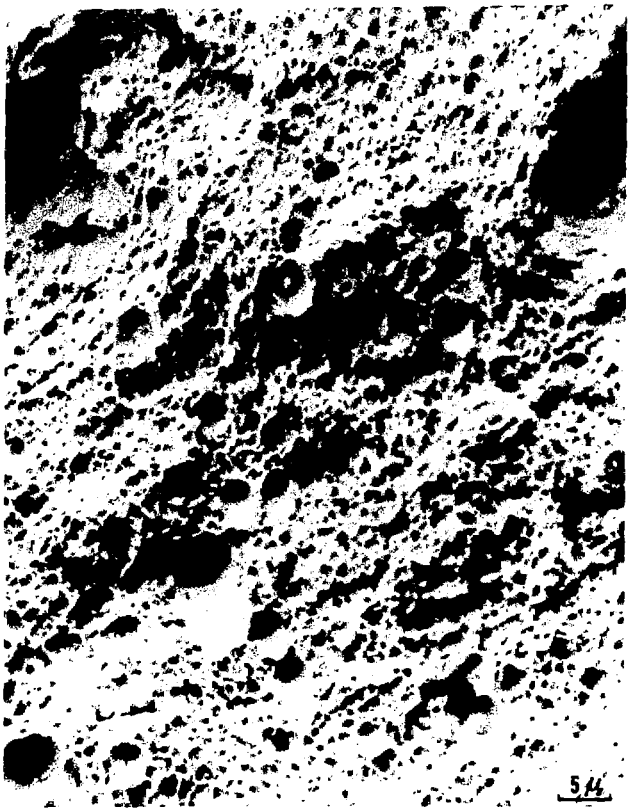

XBB 7512-9008

Fig. 19

XBB 7512-9007

Fig. 20

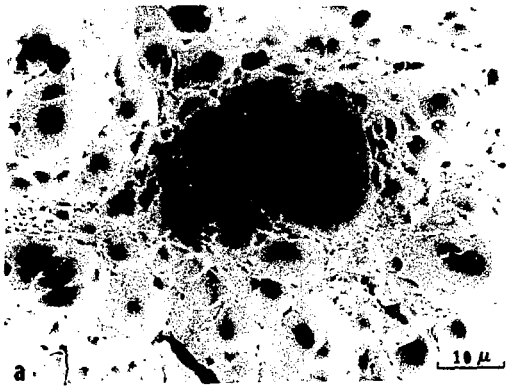

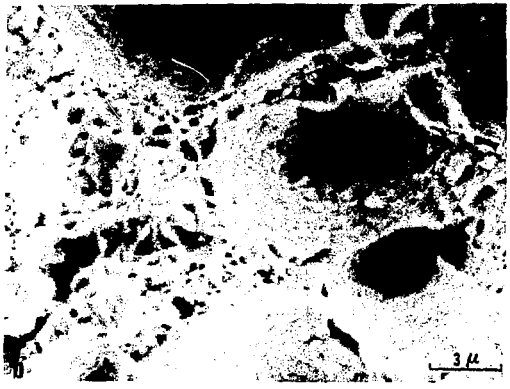

XBB 7512-9013

Fig. 21